41st Aerospace Sciences Meeting and Exhibit
6-9 January 2003, Reno, Nevada

AIAA 2003-312

Prediction of Soot Formation in a Turbulent Diffusion Jet Flame Using the Linear-Eddy Model

I. Porumbel*and S. Menon†
School of Aerospace Engineering
Georgia Institute of Technology
Atlanta, Georgia 30332

The formation of soot particles in a turbulent diffusion methane-air jet flame is predicted using the linear eddy model (LEM). A reduced mechanism with 15 reactions and 19 species for methane-air is supplemented by additional soot kinetics to compute the volume fraction and the number density of soot particles. A turbulent jet diffusion flame is simulated and compared to past experimental and numerical data reported in the literature. Comparison show that the current LEM approach is capable of predicting with reasonable accuracy, the radial and axial distribution of soot in a jet diffusion flame.

Introduction

Soot is a carbon particulate formed usually as a byproduct of incomplete hydrocarbon combustion and is typically created in fuel rich regions of the flame.[1] The impact of soot emission on the environment and also on human activity is well documented and future restrictions on emission demand that soot emission must be minimized or eliminated from combustion devices. Accurate prediction of soot production in turbulent flames will go a long way towards understanding the physics of soot production and perhaps lead to methods that can mitigate its effect.

Many past studies have investigated the mechanisms responsible for soot formation.[2,3,4] The main difficulty in predicting soot formation in diffusion flame is the complex and computationally expensive mechanism responsible for soot inception, nucleation and growth. In diffusion flames, soot is formed over a limited range of temperatures (1300 K - 1600 K)[5] and it is generally accepted that soot formation proceeds in a four - step sequence: (a) formation of precursor (gas) species, (b) particle inception and nucleation, (c) surface growth and particle agglomeration, and (d) particle oxidation. The details of each of these steps are not well known or even understood and this lack of understanding has major implication for predictive simulations.

What is reasonably known is that in the formation of precursor species[6] the most important role is played by polycyclic aromatic hydrocarbons (PAHs) which are the intermediaries between the fuel molecule and the primary soot particle. The particle inception phase involves the formation of small particles from growth by chemical means and by coagulation. Next, these particles experience surface growth and agglomeration leading to the formation of distinct objects with complex surface topology and structure. Finally, the soot particles formed in the interior of the flame can get oxidized if it passed through the flame. Past studies[2,4] have provided detailed models of all the steps, however, these detailed mechanism of soot formation is computationally very expensive, especially when turbulent flow-flame interaction is to be simulated.

In past studies, semi-empirical models have been developed[7,8,9] and used[1] to study soot formation in a jet flame. This "reduced" soot mechanism is a four-step mechanism and employed a two-equation model with transport equations for soot mass fraction and number density. The present study is aimed at predicting soot formation in turbulent diffusion methane-air jet flame using the Linear Eddy Model technique. The chemical species source terms are computed using a 19-species, 15-reactions mechanism.[10,11] Predicted soot volume fraction, flame temperature and mixture fraction are compared to experimental and numerical data[7,1] in order to validate the procedure. The effect of soot radiation on the flame temperature is estimated using a radiation model[12] based on an optically thin flame assumption.

Problem Formulation

The governing equation for the reaction - diffusion problem is:

$$\rho\frac{\partial Y_k}{\partial t} + \rho\overrightarrow{u}\cdot\overrightarrow{\nabla}Y_k - \overrightarrow{\nabla}(\rho D_k\overrightarrow{\nabla}Y_k) = \dot{\omega_k} \qquad (1)$$

where ρ is the density of the reacting mixture, $\overrightarrow{u}$ is the velocity vector and t is the time. Also, Y_k stands for each of the 20 scalars: the species mass fraction, soot number density and temperature (under the unity

*Graduate Research Assistant
†Professor, AIAA Associate Fellow

Lewis number assumption). Here, D_k is the molecular diffusion coefficient of the $k-th$ species or thermal diffusivity for the temperature equatoin, and $\dot{\omega_k}$ is the production/consumption by chemical reaction.

Equation (1) is a relationship associating instantaneous variables. If the equation is filtered, additional correlation terms requiring closure will appear. The closure problem can be avoided by using the "Linear Eddy Model" (LEM) technique.[13,14,15] In this approach, three physical processes are explicitly treated: (i)large-scale turbulent entrainment, (ii) small-scale turbulent mixing, and (iii) Reaction - diffusion at the small scales. The resolution is fine enough to resolve the smaller scales of motion (i.e., the Kolmogorov eddy, η) and thus, the reaction kinetics can be simulated without requiring any closure. The turbulent small-scale mixing models the impact of eddies in the inertial range on the scalar mixing process.

To keep the computational cost tractable while resolving the detailed kinetics, the LEM approach solves the reaction - diffusion equation (1) in a one-dimensional domain. For the jet flame of current consideration, the orientation of the line can either be axial[16,17] or radial,[18,19] depending upon what is of interest. In the present study, this line is chosen as a radial line that is convected downstream at a prescribed axial velocity to ensure mass and momentum conservation.[19] Reaction-diffusion of all scalars (Eq. 1 evolves simultaneously on this line in a deterministic manner while the effect of large- and small-scale eddies are implemented concurrently but at their respective time-scales. The effect of turbulence on the scalar field is implemented using a mapping process called block inversion[20,19] that was used in an earlier study to simulate jet flows. The size, position and the frequency of the event are determined using inertial range scaling valid for three-dimensional turbulence.

Details of this modeling approach is given elsewhere[20,19] but the earlier studies did not investigate soot formation in flames. Therefore, for completeness, the earlier model is summarized below with specific discussion of new changes implemented to simulate sooting flames.

In general, this simulation model has five major components: (i) axial large scale convection of the radial 1-D domain, (ii) large scale advection, (iii) molecular diffusion within the radial domain, (iv) turbulent convection or mixing within the radial domain, and (v) Chemical reaction and heat release effect. Each of these components are summarized below.

Axial large scale convection

The axial spreading of the jet is modelled using the jet similarity scaling law,[21] assuming a round free jet. Thus, the mean jet velocity can be decreases with the axial position as:

$$\frac{u(0)}{u(x)} = c\frac{x-x_0}{d} \tag{2}$$

with the notations in Fig.1, where the constant c in Eq. (2) was set to 0.065 based on experimental data for a round free jet, and the virtual origin of the jet, x_0 is determined as: $x_0 = -\frac{d}{c}$ where $d(x)$ is the nozzle diameter.[18] The axial variation of the velocity is shown in Fig. (2). The radial variation of the axial velocity is neglected, but the effects of the radial turbulent mixing will be taken into account, as shown later. Finally, computational time t_d and the axial position of the linear domain are related through the relationship:

$$\frac{dx}{dt} = u(x) \tag{3}$$

The computational radial domain is bounded by the jet diameter,$d = d(x)$. The jet spreading is included in the model by using the similarity relationship $d(x) = c(x - x_0)$.

In this model, the only constant that is specified is the spreading rate c. Effect of varying c has been investigated earlier[18] and it is determined that different values of c could be used to mimic other types of jet flow, e.g., confined or co-axial free jets. The present value is chosen based on past validation of this method for free jet.[18]

Large scale advection

The mean flow advection is implemented using a grid dilatation process. Since the axial velocity depends on the axial location, conservation of mass implies a radial spreading of the jet due to entrainment of the quiescent surrounding air.

McMurty et at,[22] have shown that under the low Mach number approximation the velocity gradient in a reacting flow can be written, using quantities normalized by reference quantities U_{ref}, T_{ref}, ρ_{ref} and L_{ref} as:

$$\overrightarrow{\nabla} \cdot \overrightarrow{v} = \frac{1}{\gamma \overline{p}}[\frac{\gamma \overrightarrow{\nabla} \cdot \overrightarrow{q}}{PrRe} - \frac{d\overline{p}}{d\overline{t}} + DaCe\dot{\overline{Q}}] \tag{4}$$

where $\overline{p}$ is the normalized pressure, $\overline{p} = p/\rho_{ref}R_{mix}T_{ref}$, R_{mix} is the gas constant of the mixture, γ is the ratio of specific heats, q is the heat flux vector, Pr is the Prandtl number, Re is the Reynolds number, Da is the Damkohler number, Ce is a parameter specifying the amount of heat release and $\overline{t}$ the normalized time, $\overline{t} = t/(L_{ref}/U_{ref})$.

For sufficiently large Reynolds numbers, the heat conduction term can be neglected. Also, the flow may be assumed as developing at constant pressure, so Eq. (4) simplifies to:

$$\overrightarrow{\nabla} \cdot \overrightarrow{v} = \frac{1}{\gamma \overline{p}} DaCe\dot{\overline{Q}} \tag{5}$$

Compared to the classic incompressible continuity equation,

$$\overrightarrow{\nabla} \cdot v = 0 \tag{6}$$

it can be seen that the source term in Eq. (5) accounts for the compressibility effects of the heat release.

The approach chosen for this study was to decouple the jet spreading through mass entrainment from the dilatation caused by the heat release. Thus, using Eq. (6), the radial velocity of the fuel jet can be integrated as:

$$v = -\frac{r}{2}\frac{\partial u}{\partial x} \tag{7}$$

This effect is incorporated by stretching the grid in the radial direction at a rate dictated by Eq. (7) without changing the scalar field at any grid location.

The source term in Eq. 5), that is the effect of volumetric dilatation has still to be included. Effect of heat release is an increase in temperature and since the flow is at constant pressure, this results in a decrease in density. For mass conservation, the volume of the burnt zone should increase in proportion. Although this increase is likely to be in all directions (depending upon the local flow velocity), in the present study, we are assuming that all this expansion effect can be implemented in the radial direction (i.e., there is no axial transport. This is an approximation that will be revisited later.

The above assumption the radial extent is increased for local volumetric expansion. The algorithm is described later.

Reaction-diffusion

The reaction-diffusion processes is modelled by Eq. 1, which for the present 1D domain is rewritten as:

$$\frac{\partial Y_k}{\partial t} = \frac{\dot{\omega_k} W_k}{\rho} + \frac{1}{\rho r}\frac{\partial}{\partial r}[\rho r (D_k \frac{\partial Y_k}{\partial r})] \tag{8}$$

where Y_k is the mass fraction of species k, $\dot{\omega_k}$ is the molar production rate, W_k is the molecular weight, D_k is the diffusion coefficient, and X_k is the mole fraction. Similarly, for temperature:

$$\frac{\partial T}{\partial t} = \frac{\dot{q}}{\rho} + \frac{1}{\rho r}\frac{\partial}{\partial r}(\rho r D_T \frac{\partial T}{\partial r}) \tag{9}$$

where $\dot{q}$ is the heat flux due to chemical reaction and radiation and D_T is the heat diffusion coefficient. Since radiation is an important part of the heat transfer mechanism, and soot is a highly radiative species, heat loss by radiation needs also be incorporated in the model. Kaplan et al.[12] provide a model for the radiation loss, assuming an optically thin flame. The heat loss by radiation in a methane air diffusion flame can be expressed as:

$$-\overrightarrow{\nabla} \cdot \overrightarrow{q_r} = -4a\sigma(T^4 - T_\infty^4) \tag{10}$$

where T is the local temperature, T_∞ is the ambient temperature σ is the Stefan-Boltzmann constant and a is the overall absorption coefficient of the gas:

$$a = 2.66 c_1 f_v T + 0.001(X_{CO_2} + X_{H_2O}) \tag{11}$$

where c_1 is a dimensional constant, X_k are the molar fractions of carbon dioxide and water and f_v is the soot volume fraction, computed as:

$$f_v = \frac{\rho}{\rho_{soot}} Y_{soot} \tag{12}$$

Here, the soot density, ρ_{soot} is chosen as $1800 kg/m^3$.[23] In addition to Eqs. (8) and (9) an equation similar to (1) can be written for the soot particles number density, N_C:

$$\rho\frac{\partial N_C}{\partial t} + \rho\overrightarrow{u}\overrightarrow{\nabla} N_C - \overrightarrow{\nabla}(\rho D_N \overrightarrow{\nabla} N_C) = \dot{\omega_N} \tag{13}$$

If the number density "diffusion" D_N coefficient is set to zero and the convective terms are neglected as for the species Eqs. (1), Eq. (13) can be written as:

$$\frac{\partial N_C}{\partial t} = \dot{\omega_N} \tag{14}$$

where the source term $\dot{\omega_N}$ is computed as described in section 2.5.

Radial turbulent convection

Turbulent convection (or stirring) is simulated by a stochastic procedure that interrupts the numerical solution of Eqs. (8) and (9), modelling the effect of a turbulent eddy on the scalar field. Thus, turbulent mixing is incorporated as a mapping process of the scalar field. There are three elements requiring specification in order to implement the mapping, characterizing the random turbulent eddy: the eddy size, the eddy location and the frequency of the mapping event. While the eddy size and location are randomly chosen using numerical techniques to be described in the next section, the frequency is determined based on inertial range scaling laws. Earlier studies[20,19] have shown that stirring frequency is given by:

$$\lambda = \frac{\nu}{d(x)^3}[\frac{d(x)}{\eta}]^{\frac{4}{3}} \frac{[\frac{d(x)}{\eta}]^{\frac{5}{3}} - 1}{1 - [\frac{\eta}{d(x)}]^{\frac{4}{3}}} \tag{15}$$

where ν is the kinematic viscousity of the mixture, such that the mapping timescale is:

$$\tau_{stir}(x) = c_\tau(\lambda d(x))^{-1} \tag{16}$$

where c_τ is a calibration constant, set to 15 in this study based on a earlier study.[24]

Chemical mechanism

Here, a well established reduced reaction mechanism for methane-air[11] has been used in the past.[10] Starting from a detailed mechanism consisting of 277 reactions and 48 species, a reduced mechanism consisting of 15 reactions and 19 species is developed. The 19 tracked species are H_2, H, O_2, OH, H_2O, CH_3, CH_4, CO, CO_2, CH_2O, C_2H_2, C_2H_4, C_2H_6, N_2, HO_2, H_2O_2, NO, HCN, NH_3. To these species, soot adds another species. The reaction rates are as defined earlier for the gas phase mechanism, but we need a mechanism for the soot processes.

Kronenburg at al.[1] present a semi - empirical model consisting in a four - step global mechanism for soot formation based on the models developed earlier.[7,8,9]

$$C_2H_2 \rightarrow^n 2C + H_2 \tag{17}$$

$$C_2H_2 \rightarrow^g 2C + H_2 \tag{18}$$

$$C + \frac{1}{2}O_2 \rightarrow CO \tag{19}$$

$$C + OH \rightarrow CO + H \tag{20}$$

Here, these reactions represent respectively, the soot soot particle nucleation (step 1 in the above mechanism), the particle growth (step 2) and soot oxidation (steps 3 and 4). The reaction rates for each of these steps are given by:[1]

$$r_1 = k_1(T)[C_2H_2] \tag{21}$$

$$r_2 = k_2(T)A_s[C_2H_2] \tag{22}$$

$$r_3 = k_3(T)A_s[O_2] \tag{23}$$

$$r_4 = k_4(T)A_s[OH] \tag{24}$$

where $[C_2H_2]$, $[O_2]$ and $[OH]$ are the concentrations of ethylene, molecular oxygen and hydroxyl A_s is the soot surface area per unit volume and the reaction rate constants are computed using the Arrhenius law (with the coefficients in Table 1):

$$k = AT^b e^{-\frac{T_\infty}{T}} \tag{25}$$

The soot surface area per unit volume can be expressed as:[1] $A_s = \pi d_p^2 \rho N_C$, where N_C is the soot number density and d_p is the average soot particle diameter:

$$d_p = (\frac{6}{\pi}\frac{\rho}{\rho_{soot}}\frac{Y_C}{\rho N_C})^{\frac{1}{3}} \tag{26}$$

Thus, the source terms for the soot mass fraction equation is:[1]

$$\dot{\omega_C} = 2r_1 + 2r_2 - r_3 - r_4 \tag{27}$$

while for the soot number density is:

$$\dot{\omega_N} = 2r_1\frac{N_A}{n_{C,min}} - 2C_a\sqrt{d_p\frac{6\sigma_B T}{\rho_{soot}}}(\rho N_C)^2 \tag{28}$$

where the negative term accounts for the decrease in number density due to particle aggregation[1] and $\sigma_B = 1.38 \times 10^{-23}$ J/K is the Boltzmann constant, $N_A = 6.0232 \times 10^{26}$ is the Avogadro number, $C_a = 9$ is the agglomeration constant and $n_{C,min} = 60$ is the minimum particle number required for particle nucleation.

Numerical Method

The numerical method is identical to the approach employed in the past to study aerosol dynamics in jet plumes[19] and is based on the earlier development[20,18] and is modified here to include soot formation and radiation effects. The code numerically integrates the scalar Eqs. (8), (9) and (14) using a second-order finite difference scheme. The time step for the reaction-diffusion equations, Δt_{LEM} is determined by the minimum of the diffusion time step t_{dif} and a chemical time step t_{chem}. The CHEMKIN package[25] is employed for the time integration of the reaction rate mechanism. The soot diffusion coefficient was set to zero, following the work of Kronenburg et al.[1]

At the same interval, Δt_{LEM}, the grid is dilated radially to account for mass conservation. There are two parts to this stretching of the grid. The grid is stretched to account for the axial spreading of the jet and to account for volumetric heat release. The volume change associated with the increase in temperature is computed at each time step as:

$$\Delta V_i^n = \frac{\rho_i^{n-1}\Delta V_i^{n-1}}{\rho_i^n} \tag{29}$$

where ΔV is the volume of a computational cell, i is the current radial position, n the current time step and $n-1$ the previous time step. Since the numerical method is one dimensional, the change in volume will occur only in the radial direction and therefore, the increase in the radial dimension of a cell will be:

$$\Delta r_i^n = \frac{\rho_i^{n-1}\Delta r_i^{n-1}}{\rho_i^n} \tag{30}$$

and the new radial position of the cell:

$$r_i^n = \sum_{j=i_0}^{i-1} r_i^n + \frac{\Delta r_i^n}{2} \tag{31}$$

where i_0 corresponds to the centerline, $r = 0$.

The thermal expansion as modeled above results in non-uniform grid spacing due to radial variation in heat release. However, for the turbulent stirring implemented here, it is beneficial to keep all the cells to equal size. Therefore, a re-gridding is carried out. This

re-gridding can cause some spurious diffusion in some cells but it is considered negligible since the current resolution is very high.

Concurrently to the reaction-diffusion and thermal expansion processes described above, at time intervals based on the stirring frequency (16), the turbulent mixing process interrupts the integration process through an instantaneous mapping event. First, an eddy size l is randomly chosen from a power law distribution within the range $\eta < l < L(x,r)$, where η is the Kolmogorov scale:

$$\eta = KRe^{-\frac{3}{4}} \tag{32}$$

K is a proportionality constant and $L(x,r)$ is the integral length scale. The constant K was set in this case equal to the value suggested by Menon and Wu,[18,19] $K = 2.83$. The PDF is determined from inertial range scaling laws as:[18]

$$f(l) = \frac{5}{3L(x,r)} \frac{1}{[\frac{L(x,r)}{\eta}] - 1} [\frac{l}{L(x,r)}]^{-\frac{8}{3}} \tag{33}$$

The largest eddy size L(x, r) is a function of the local jet diameter:

$$L(x,r) = \begin{cases} d(x) & |r| < \frac{d(x)}{2} \\ 2[d(x) - |r|] & |r| \geq \frac{d(x)}{2} \end{cases} \tag{34}$$

As shown earlier,[18] Eq. (16) ensures that eddies within the jet shear layer are the ones that are picked for stirring. Next, the center of the eddy, r0, is randomly chosen within the radial domain using a bimodal Gaussian distribution function:

$$G(r_0) = \pm[\sigma X + r_j(x)] \tag{35}$$

where X is a standard normally distributed random variable, $r_j(x)$ is the current jet radius and σ is the distribution variance. In the present study, the variance was chosen equal to the current jet diameter, $d(x)$, thus yielding a nearly uniform distribution within the jet and smoothly decaying outwards.

A bimodal distribution was chosen because the turbulence intensity peaks in the shear layer surrounding the jet so the maximum probability for turbulent eddies occurrence should be at the jet edge. In the far field the two shear layers grow and eventually merge so the eddies have an uniform probability to occur inside the jet. The chosen distribution seeks to model both these phenomena without the need for changing the pdf as the jet evolves. However, the bi - modal Gaussian distribution is not an exact model in either region (near or far field) and it may cause inaccuracies in the results.

Once the eddy and the eddy size are known, a rearrangement of the scalar fields contained within the eddy length, called block inversion,[13] takes place. Thus, all scalar fields $Y_k(r,t)$ in the range $r_0 - l/2 < r < r_0 - l/2$ are replaced by the scalar fields $Y_k(2r_0 - r, t)$, causing a rotation by 180° of the scalar fields.

Subsequently, molecular diffusion smoothes out the sharp gradients caused by the block inversion and, thus, both molecular diffusion and turbulent mixing play a competitive role in the process. Because the cell physical volume expand with the radial location, the block inversion would cause mass conservation errors. To correct for that, the mapping of scalars from cell 'a' to cell 'b' is made through the relationship:

$$Y_b^{new} = \frac{(\rho_a Y_a - \rho_b Y_b)V_a + \rho_b Y_b V_b}{(\rho_a - \rho_b)V_a + \rho_b V_b} \tag{36}$$

The process is, then, continued at the next axial location, related to the time step through Eq. (3) and carried on until the outflow boundary is reached. Multiple (typically 50) realizations of the flow are ensemble-averaged to obtain the statistically significant mean fields.

Results and Discussion

The computations are carried out for a round jet of fuel (methane) of diameter 4.07 mm, with an exit velocity of 20.3 m/s, surrounded by quiescent air. The resulting Reynolds number is about 5,000. The initial temperature of the fuel and that of the surrounding air was 290 K. The combustion process was assumed as taking place at the atmospheric pressure. The results of this study are compared to the numerical results provided by Kronenburg et al.[1] and to the data reported by Brookes et al.[7]

The computational grid is uniform with a spacing of 0.01 mm which is of the same order of magnitude as the Kolmogorov scale. The actual number of grid used to resolve the radial line at a given axial location depends upon the resolution needed to resolve the Kolmogorov eddy and the extent of the jet. Therefore, as the line moves downstream, the number of grid cells increase both due to spreading and due to volumetric expansion. For statistical stationary estimates, 50 realizations of the flow are performed and time-averaged.

The duration of the computation of one flow realization up to x = 300 mm is 100 hours on a 1.2 GHz Pentium 4 Xeon machine using the direct integration of the chemical reaction rates.

Figure 3 shows the radial temperature profile at 150 mm downstream of the nozzle. The agreement with the measured data[7] is reasonable. The slight under prediction of the peak temperature and the slight over prediction of the centerline temperature indicates that the turbulent mixing rate, controlled by the jet spreading constant c_τ in Eq. (16) is slightly overestimated. However, the peak location is well predicted in the present study. In contrast, the peak is shifted up-

stream in the earlier study[1] and their prediction is consistently below the measured data.

As shown in Fig. (3), the flame front is located around r = 10 mm and the centerline region of the jet is not yet fully ignited due to the lack of oxygen. As expected, the carbon monoxide mass fraction peaks in the same region. On the other hand, both the product species (CO_2 and H_2O) have higher values at the centerline than at the flame. This is explained by noting that the higher temperature at the front flame triggers the dissociation of both water and carbon dioxide molecules, thus decreasing the mass fraction of CO_2 and H_2O.

At a distance x = 250 mm (Fig. 5), the temperature is over predicted across the flame by approximately 15 percent (while it is underpredicted in the earlier study.[1] The present over prediction may be the effect of the underestimation of the heat loss by radiation. The current model assumes an optically thin flame and the assumption has decreasing validity as the soot volume fraction and particle size increases downstream of the flame.

The major species profiles at this axial distance of 250 mm are shown in Fig. 6. The product species have high mass fraction across the jet indicated that the reactions are close to completion, although there is still some fuel present at this location.

The radial profile of the soot volume fraction at different distances from the burner exit are presented in Figs. 7 - 9. Generally, they show a better agreement with the experimental data than the previous study[1] using the same semi-empirical soot mechanism. The maximum soot volume fraction matches the experimental data at $x = 150mm$ well but occurs inside the flame closer to the centerline than measured. This may be a flaw of the semi - empirical model used to model the soot chemistry, since the same tendency is shown by the numerical results obtained by Kronenburg at al.[1] (although they show a significant over prediction of peak value). Closer to the centerline, the soot volume fraction is overpredicted in the present study, and this is consistent with the higher centerline temperature shown in Fig. (7).

In the regions outside of the flame the temperature is low and soot production is not significant yet. Also, turbulent mixing decreases away from the shear layer due to decrease in turbulent intensity. Therefore, the presence of soot in this region is primarily a molecular diffusion effect. The underprediction at large values of r may be because soot diffusion is neglected. On the hand, it is shown by Kronenburg et al.,[1] using the same diffusion coefficient for soot as for the gaseous species leads to a gross underestimation of the peak soot volume fraction. Therefore, this issue remains unresolved.

Further downstream (Fig. 8), the soot volume fraction shows an improved agreement with the experimental data. The same tendency was observed by Kronenburg et al.,[1] this suggests that the soot semi-empirical mechanism is optimal in this region. The peak soot volume fraction occurs now at the centerline but there is slight over prediciton. At $x = 250mm$, the soot volume fraction (Fig. 9) is over predicted due to the over prediction of the temperature profile. Another reason for the prediction of significant quantities of soot at large radii may be the inaccuracy of the distribution function (Gaussian) used for determining the location of the turbulent eddies.

The centerline axial profiles of temperature and soot volume fraction are presented in Figs. 10 and 11. The axial temperature growth rate is well predicted although there is a slight over prediction. This is also reflected in the soot profile.

Finally, Figs. (12) and (13) show the normalized (using scale-similar variables) radial profiles of temperature and soot volume fraction, respectively, at three different axial distances from the nozzle where T_0 is the maximum temperature and f_v0 is the maximum soot volume fraction at each location and $r(x)$ is the jet radius at position x. The temperature profiles become self similar around an axial distance $x/d = 40$ and the soot volume fraction also show a similar tendency, even if not with the same accuracy.

Conclusions

The LEM technique proved to be a useful and computationally efficient method to model turbulent scalar mixing in canonical flows. In this study, it has been used to simulate jet diffusion flame with soot dynamics included. The sooting flame simulated here is identical to a flame studied both experimentally and numerically using e semi-empirical soot model.[1] Comparisons with these results show that the present calculation predicted quite well the overall trend and in some cases, the magnitude of the temperature and soot volume fraction in the jet flame. Some discrepancies are also observed and the possible reasons for this have been discussed. In any event, these calculations show that complex physics in jet flames can be approximated quite well using the LEM approach. Since the domain is reduced to 1D the overall cost of the simulation is dictated by the number of realizations used for statistics and the cost of computing the chemistry. For this reduced mechanism, the chemistry evaluation is still a major overhead but this can be reduced considerably by using In-Situ Adaptive Tabulation (ISAT)[26] or Artificial Neural Network (ANN)[27] which have been shown to reduce chemistry update cost by orders of magnitude.

Two important calibration constants control the process, the jet spreading rate c in Eq. 2, set to 0.065 determining how far the flame develops radially and the eddy frequency constant c_τ in Eq. 16, set to 15, determining the intensity of the turbulent mixing.

The interplay of these two constants, together with the distribution function chosen for the occurrence of the turbulent eddy (Eq. 35) determines the accuracy of the numerical results. The sensitivity of the predictions to these parameters still remain to be addressed and will be the topic of a future study.

Acknowledgments

This work is supported in part by Army Research Office and General Electric Power Systems. High Performance Computing (HPC) resources are provided by the Department of Defense (DOD) Major Shared Resources Centers (MSRC) at Naval Oceanographic Office (NAVOCEANO), and ERDC (AL).

References

[1] Kronenburg, A., Bilger, R., and Kent, J., "Modeling Soot Formation in Turbulent Methane - Air Jet Diffusion Flames," *Combustion and Flame*, Vol. 121, 2000, pp. 24–40.

[2] Kazakov, A. and Frenklach, M., "Dynamic Modeling of Soot Particle Coagulation and Aggregation: Implementation With the Method of Moments and Application to High - Pressure Laminar Premixed Flames," *Combustion and Flame*, Vol. 114, 1998, pp. 484–501.

[3] Frenklach, M. and Harris, S., "Aerosol Dynamisc Modeling Using the Method of Moments," *Journal of Colloid and Interface Science*, Vol. 118, No. 1, 1987.

[4] Frenklach, M. and Wang, H., "Detailed Modeling of Soot Particle Nucleation and Growth," *Twenty - Third Symposium (International) on Combustion*, 1990, pp. 1559–1566.

[5] Turns, S., *An Introduction to Combustion: Concepts and Applications*, The McGraw - Hill Companies, 1999.

[6] Glassman, I., "Soot Formation in Combustion Processes," *Twenty - Second Symposium (International) on Combustion*, 1988, pp. 295–311.

[7] Brookes, S. and Moss, J., "Measurements of Soot Production and Thermal Radiation from Confined Turbulent Jet Diffusion Flames of Methane," *Combustion and Flame*, Vol. 116, 1999, pp. 49–61.

[8] Brookes, S. and Moss, J., "Predictions of Soot and Thermal Radiation Properties in Confined Turbulent Jet Diffusion Flames," *Combustion and Flame*, Vol. 116, 1999, pp. 486–503.

[9] Lindstedt, P., "A Reaction Mechanism for Soot Formation in Non-Premixed Flames," *Proceedings of the IUTAM Symposium on Aerothermodynamics in Combustors*, 1992, pp. 145–158.

[10] Kapoor, R., Lentati, A., and Menon, S., "Simulations of Methane - Air Flames Using ISAT and ANN," *AIAA Paper No. 01-3847*, 2001.

[11] Chen, J.-Y., Private Communication.

[12] Kaplan, C., Shaddix, C., and Smyth, K., "Computations of Enhanced Soot Production in Time - Varying CH4 / Air Diffusion Flames," *Combustion and Flame*, Vol. 106, 1996, pp. 395–405.

[13] Kerstein, A. R., "Linear-Eddy Model of Turbulent Transport II," *Combustion and Flame*, Vol. 75, 1989, pp. 397–413.

[14] Kerstein, A. R., "Linear-Eddy Modeling of Turbulent Transport. Part 6. Microstructure of Diffusive Scalar Mixing Fields," *Journal of Fluid Mechanics*, Vol. 231, 1991, pp. 361–394.

[15] Kerstein, A. R., "Linear-Eddy Modeling of Turbulent Transport. Part V: Geometry of Scalar Interfaces," *Physics of Fluids A*, Vol. 3, No. 5, 1991, pp. 1110–1114.

[16] Menon, S. and Jou, W.-H., "Large-Eddy Simulations of Combustion Instability in an Axisymetric Ramjet Combustor," *Combustion Science and Technology*, Vol. 75, 1991, pp. 53–72.

[17] Calhoon, W. H. and Menon, S., "Comparison of Reduced and Full Chemical Mechanisms for NOx Prediction in Non-Premixed Turbulent H2-Air Jet Flames," *AIAA-94-0676*, 1994.

[18] Menon, S. and Wu, J., "Effects of Micro- and Macroscale Turbulent Mixing on the Chemical Processes in Engine Exhaust Plumes," *Journal of Applied Meteorology*, Vol. 37, 1998, pp. 639–653.

[19] Wu, J. and Menon, S., "Aerosol Dynamics in the Near Field of Engine Exhaust Plumes," *Journal of Applied Meteorology*, Vol. 40, 2001, pp. 795–809.

[20] Menon, S., Calhoon, W., Goldin, G., and Kerstein, A., "Effects of Molecular Transport on Turbulence Chemistry Interactions in a Hydrogen-Argon-Air Jet Diffusion Flame," *Twenty - Fifth Symposium (International) on Combustion*, 1994, pp. 1125–1131.

[21] Landau, L. and E.M., L., *Turbulence. Fluid Mechanics*, Pergamon Press, 1959.

[22] McMurtry, P. A., Riley, J. J., and Metcalfe, R. W., "Effects of Heat Release on the Large-Scale Structure in Turbulent Mixing Layers," *Journal of Fluid Mechanics*, Vol. 199, 1989, pp. 297–332.

[23] Stewart, C., Syed, K., and Moss, J., "Modeling Soot Formation in Non - premixed Kerosene - Air Flames," *Combustion Science and Technology*, Vol. 75, 1991, pp. 211–226.

[24] Smith, T. and Menon, S., "One-dimensional simulations of freely propagating turbulent premixed flames," *Combustion Science and Technology*, Vol. 128, 1996, pp. 99–130.

[25] Kee, R., Rupley, F., and Miller, J., "CHEMKIN-III A Fortran Chemical Kinetics Package for the Analysis of Gas Phase Chemical Kinetics," Tech. Rep. SAND96-8216, Sandia National Laboratories, 1996.

[26] Pope, S., "Computationally Efficient implementation of combustion chemistry using in situ adaptive tabulation," *Combustion Theory Modelling*, Vol. 1, 1997, pp. 41–63.

[27] Kapoor, R., *Artificial Neural Networks for Efficient Kinetics Modeling in Turbulent Reacting Flows*, Ph.D. thesis, Proposal, Georgia Institute of Technology, Atlanta, GA, August 2002.

Reaction	A	b	T_∞
1	$0.63x10^4$	0	21000
2	$0.75x10^3$	0	12100
3	$7.15x10^2$	1/2	19800
4	0.36	1/2	0

Table 1: Reaction rate constants for the soot mechanism

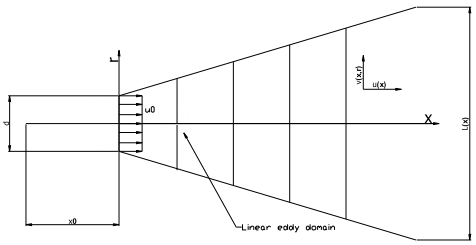

Fig. 1 Computational domain (not to scale).

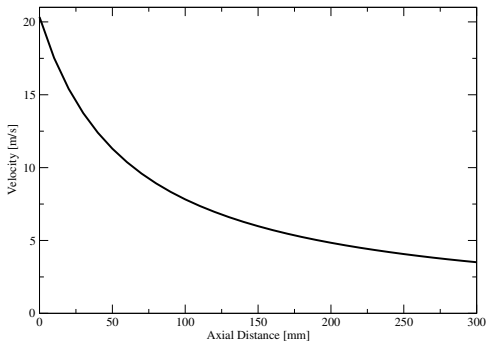

Fig. 2 Velocity axial decay.

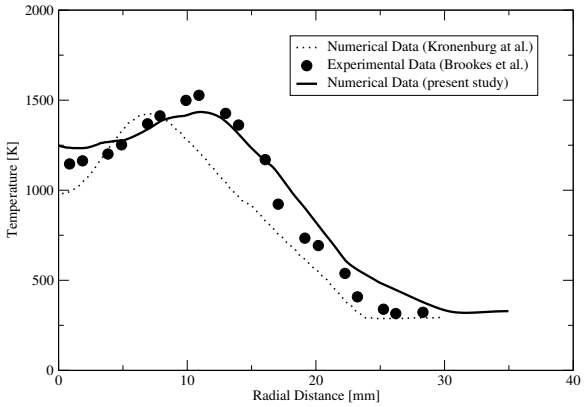

Fig. 3 Radial temperature profile at x = 150 mm. The symbols represent measured temperatures, the continuous line indicates the results of the present study and the dotted line is the numerical results of Kronenburg et al.[1]

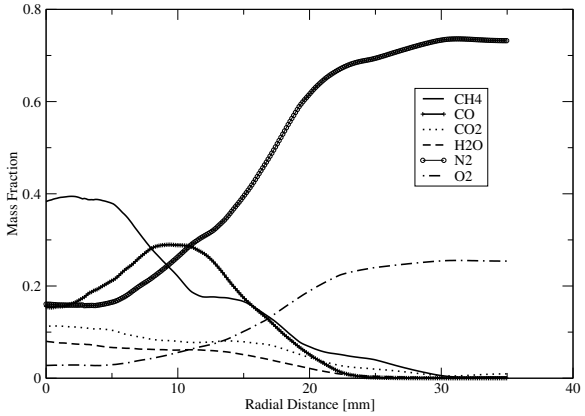

Fig. 4 Radial Mass fraction profiles of the major species At x = 150.

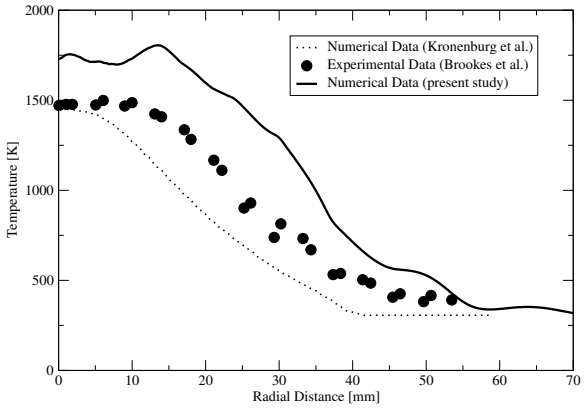

Fig. 5 Radial temperature profile At x = 250 mm.

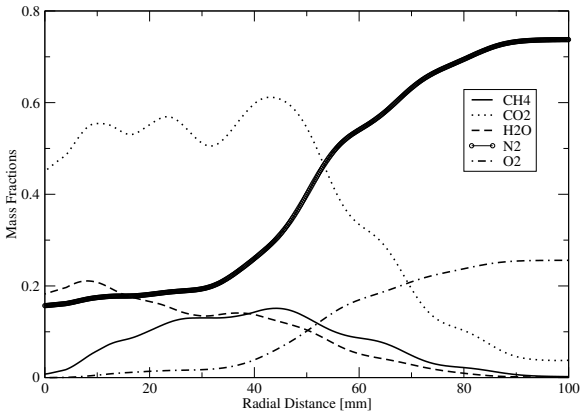

Fig. 6 Radial mass fraction profiles of the major species At x = 250.

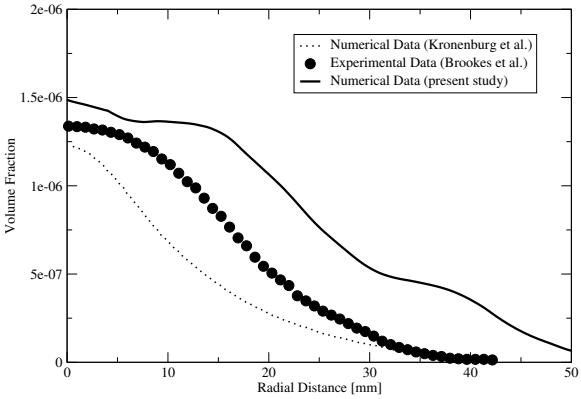

Fig. 9 Radial soot volume fraction profile At x = 250.

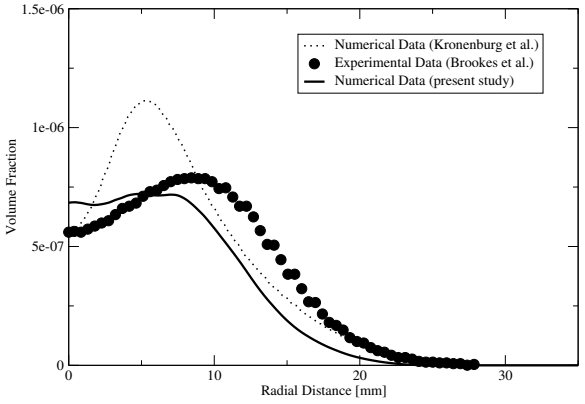

Fig. 7 Radial soot volume fraction profile at x = 150.

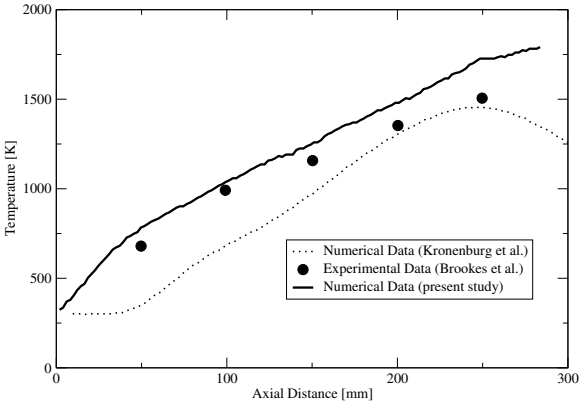

Fig. 10 Axial temperature profile.

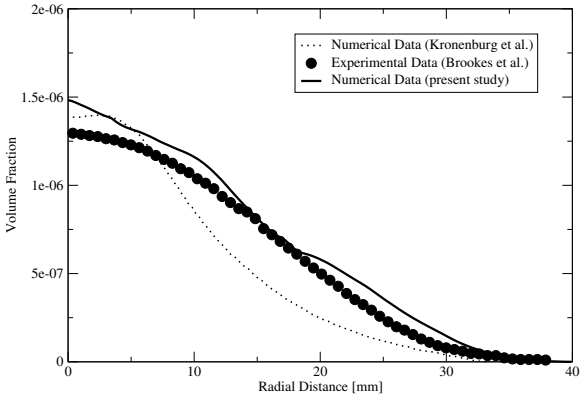

Fig. 8 Radial soot volume fraction profile At x = 200.

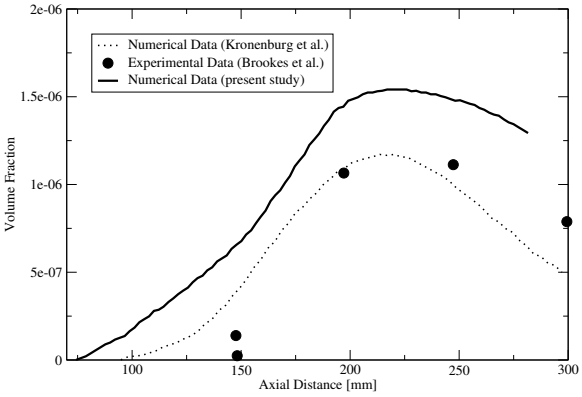

Fig. 11 Axial soot volume fraction profile.

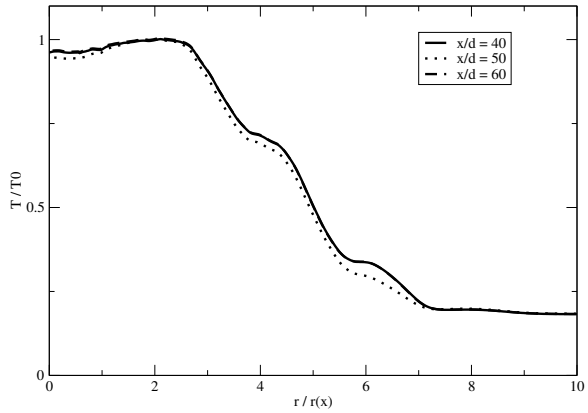

Fig. 12 Normalized radial temperature profiles.

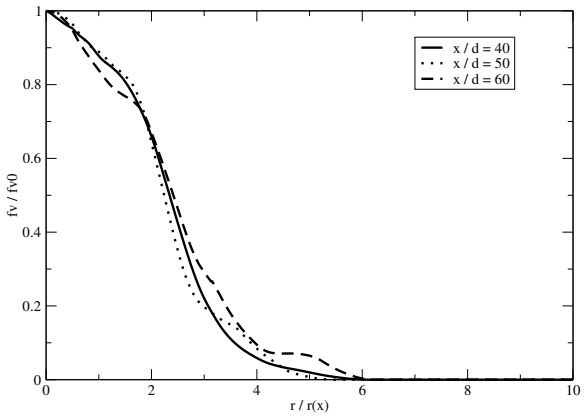

Fig. 13 Normalized radial soot volume fraction profiles.